CRUSTAL STRUCTURE OF THE ZIMBABWE CRATON AND THE LIMPOPO BELT OF SOUTHERN AFRICA: NEW CONSTRAINTS FROM SEISMIC DATA AND IMPLICATIONS FOR ITS EVOLUTION

J. GORE
Department of Physics, University of Zimbabwe, Box MP 167, Mt Pleasant, Harare, Zimbabwe,
School of Geosciences, University of Witwatersrand, Wits 2050, Johannesburg, South Africa
CTBTO PrepCom, Vienna International Centre, P.O. Box 1200, 1400 Vienna, Austria
e-mail: Jane.Gore@CTBTO.ORG

D.E. JAMES
Department of Terrestrial Magnetism, Carnegie Institution of Washington, 5241 Broad Branch Road, N.W., Washington, 20015 DC, United States of America
e-mail: james@dtm.ciw.edu

T.G. ZENGENI
Department of Physics, University of Zimbabwe, Box MP 167, Mt Pleasant, Harare, Zimbabwe,
e-mail: zengeni@science.uz.ac.zw

O. GWAVAVA
Department of Physics, University of Zimbabwe, Box MP 167, Mt Pleasant, Harare, Zimbabwe
Department of Geology, University of Fort Hare, Private Bag X1314, Alice 5700, South Africa
Corresponding author
e-mail: ogwavava@ufh.ac.za

ABSTRACT

Teleseismic data recorded by twenty two northern stations of the Southern Africa Seismic Experiment (SASE) have been analysed to map the crustal and uppermost mantle structure of the Zimbabwe Craton and the Limpopo Belt. The results show that the crustal thickness of the Limpopo Belt ranges from 42 to 53 km with a complex Moho, while that of the Zimbabwe Craton ranges from 36 to 39 km, with a relatively sharp and simple Moho and no apparent mid-crustal discontinuities. Poisson's ratio estimates show the crust under the Limpopo Belt to be of a relatively more mafic composition ($\sigma > 0.26$) than under the Zimbabwe Craton ($\sigma \leq 0.26$), which is of intermediate composition.

Introduction

Controversy still surrounds the origin and relation of the Limpopo Belt in southern Africa, perhaps the best-known Archaean "mobile" belt in the world, to the adjacent Archaean Zimbabwe and Kaapvaal Cratons. Many models have been proposed to try and explain how the Limpopo Belt originated. Some models propose continent-continent collision between the Zimbabwe and Kaapvaal Cratons, while some propose a non-plate tectonic origin. Of interest is the fact that those models that propose continent-continent collision between the two cratons do not agree on the timing of such an event. Ages of both ~2.6 to ~2.7 Ga (e.g. McCourt and Armstrong, 1998) and ~2.0 Ga (e.g. Holzer *et al.*, 1998) events have been found for the Limpopo Belt, which makes it difficult to attach a single date for the collision. Kamber *et al.* (1995a; 1995b) argue that because of pervasive evidence for 2.0 Ga events, there is little basis for assuming that the Limpopo Belt is necessarily a product of late Archaean collision between the two cratons.

According to Bleeker (2003) it seems that the Zimbabwe and Kaapvaal Cratons do not share any history prior to ~2.0 Ga due to major differences in structure, time of cratonisation and mafic dyke swarms among others. He further asserts that the Great Dyke, dated to be ~2.6 Ga (Mukasa *et al.*, 1998) does not cross the Limpopo Belt into the Kaapvaal Craton, hence the two cratons could only have collided around 2.0 Ga. Nonetheless, the dyke does extend into the Northern Marginal Zone of the Limpopo Belt, suggesting that it may postdate the tectonic event that produced the Limpopo Belt. If the age of the Limpopo Belt as a collisional terrain is resolved, then this may help answer the question of whether or not plate tectonic processes acting in the Archaean are comparable to those in the Proterozoic.

While it is necessary to interpret geological and geophysical data simultaneously in order to come up with a comprehensive evolutionary picture, much of the geophysical work carried out on the Zimbabwe Craton and the Limpopo Belt did not serve to provide vital

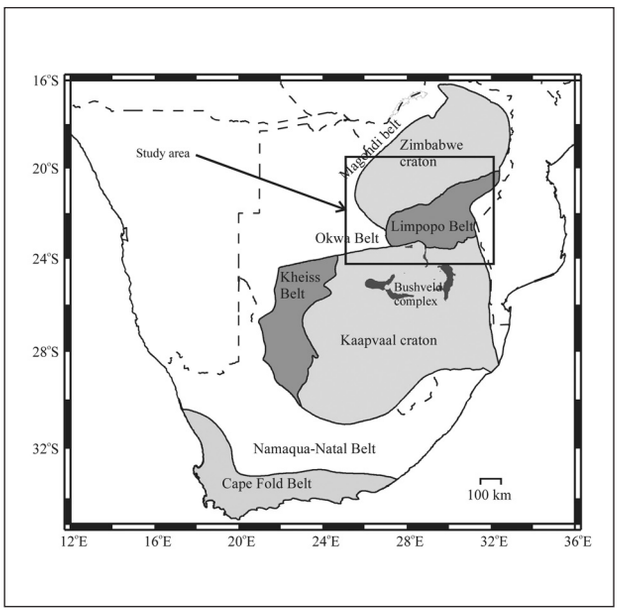

Figure 1. *Geological setting of the study area.*

constraints. Most of the work only probed the shallow crustal structure, while a few studies provided the depth to the Moho, but did not indicate the nature of the Moho discontinuity structure. Seismic studies managed to provide average crustal P-wave velocities without any estimates of average Poisson's ratios, vital for differentiating felsic from mafic rocks. There have been some disagreements about whether the lower crusts of Archaean cratons are mafic or not. Some workers have suggested that Archaean crust is more mafic than Proterozoic crust (e.g. Zandt and Ammon, 1995) while some believe it is less mafic (e.g. Durrheim and Mooney, 1991; Niu and James, 2002; James et al., 2003). Information on the composition of the lower crust is vital in the quest for an answer to processes of Archaean crustal formation, hence the need to establish Poisson's ratio estimates.

The aim of this paper is to provide new constraints on the crustal and uppermost mantle seismic structure of the Zimbabwe craton and the Limpopo Belt from receiver function analysis that can be used to try to constrain some proposed models on the crustal evolution of the Limpopo Belt.

Geological setting of the study area

The study area lies roughly between 19°S and 24°S, 25°E and 32°E and comprises the southern part of the Zimbabwe Craton, the Limpopo Belt, the eastern-most part of the Okwa and Magondi Belts and the northern-most part of the Kaapvaal Craton (Figure 1).

The Zimbabwe Craton is comprised chiefly of granites and gneisses with relatively small, irregularly-shaped inclusions of greenstone belts, with ages that range from 3.5 to 2.6 Ga (Blenkinsop et al., 1997). The formation of the Zimbabwe Craton is considered to have occurred in two distinct episodes, the first circa 3.8 to 3.2 Ga, involving the formation of the early

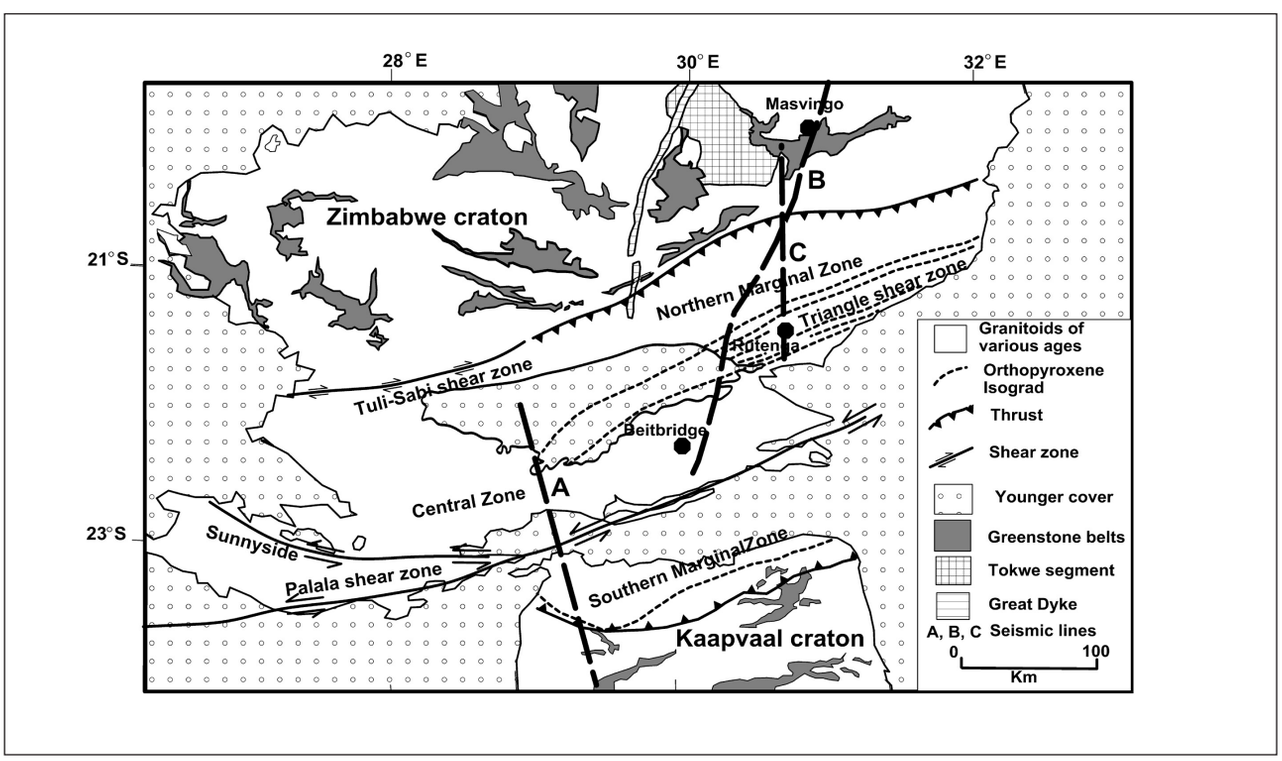

Figure 2. *Geological map of the Limpopo Belt (after Rollinson, 1993).* ***A*** *= seismic reflection profile of Durrheim et al. (1992).* ***B*** *= seismic refraction profile of Durrheim et al. (1992).* ***C*** *= seismic refraction profile of Stuart and Zengeni (1987).*

cratonic nucleus and a second circa 3.0 to 2.6 Ga, involving magma genesis and crustal formation (Horstwood et al., 1999). This is similar to the formation of the Kaapvaal Craton, also thought to be formed in two stages, at circa 3.64 to 3.08 Ga and 3.0 to 2.6 Ga (Brandl and De Wit, 1997). Growth of the lithospheric mantle beneath Zimbabwe at ~3.8 Ga is in agreement with Re-Os results of Nägler et al. (1997). The final stabilisation or cratonisation of the Zimbabwe Craton is believed to have been completed at ~2.6 Ga (Wilson, 1990; Horstwood et al., 1999). At the end of stabilisation, the first major igneous event was the intrusion of the Great Dyke and its satellites at circa 2.575 58 Ga (Mukasa et al., 1998; Armstrong and Wilson, 2000).

The Limpopo Belt is situated between the Zimbabwe and Kaapvaal Cratons (Figure 1). It is approximately 700 km long, ranging in width from 240 to 320 km, with an area of about 185 000 km^2. Kalahari sands cover the western reaches of the Limpopo Belt in Botswana, while to the east the Belt is obscured by Proterozoic and Phanerozoic sedimentary cover. Any possible extension further east has been masked by the Pan-African Mozambique Belt (Key and Hutton, 1976).

The Limpopo Belt consists of three zones (Figure 2) based on structural signature (Cox et al., 1965): the northern and southern Marginal Zones and the Central Zone. The Northern Marginal Zone (NMZ) lies within Zimbabwe with structural fabric trending east-northeast to west-southwest (Mkweli et al., 1995). Rocks of the NMZ consist of high-grade metamorphic equivalents of the flanking Archaean granite-greenstones of the Zimbabwe Craton (Rollinson, 1993; Rollinson and Blenkinsop, 1995). The NMZ has been subdivided by some workers into the Transition Zone and the Triangle shear zone (Rollinson and Blenkinsop, 1995). The Triangle shear zone, which defines the boundary between the NMZ and the Central Zone (CZ), is related to the Tuli-Sabi shear zone (Mkweli et al., 1995). The Southern Marginal Zone (SMZ) lies within South Africa (Figure 2) and comprises high-grade metamorphic equivalents of the flanking Archaean granite-greenstone terrains (Du Toit et al., 1983; Kreissig et al., 2000) of the Kaapvaal Craton. The Sunnyside-Palala shear zone forms the boundary between the SMZ and the CZ.

Besides having similar petrology and contact relationships with the adjacent cratons along major thrust systems (Van Reenen et al., 1995), these two marginal zones share other important similarities. Both zones are believed to have been thrust over the adjoining cratons at approximately 2.6 to 2.7 Ga (Kamber et al., 1995b), and there is evidence that they both underwent metamorphism at around 2.0 Ga (Kamber et al., 1995a; 1995b; Schaller et al., 1999).

The CZ is situated between the two marginal zones, Figure 2, with folds that trend almost northerly (Watkeys, 1983). The CZ is bounded to the north by the Triangle shear zone and in the south by the Palala shear zone. Rocks in the CZ are dominated by high-grade paragneisses and metasediments as well as layered igneous complexes with rare intrusive granites (Watkeys et al., 1983). A possible explanation to the origin of the high-pressure grade rocks is that the crust of the CZ was thickened down to depths of 60 to 70 km at about 2.7 Ga, as a result of continent-continent collision (Van Reenen et al., 1987). It then had 20 to 30 km of its upper crust exhumed, as indicated by relict kyanite inclusions in garnets, leaving high pressure metamorphic assemblages at the surface (Van Reenen et al., 1987).

Data

Data acquisition started in April 1997 in the Southern Africa Seismic Experiment and ended in April 1999. At any one time an array of the available 56 portable broadband earthquake monitoring systems (seismic stations) was deployed. A total of 82 distinct sites were ultimately occupied by portable seismographs. The orientation and configuration of the recording sites were arranged optimally to capitalise on the preferred sources from the known distribution of global seismicity and to maximise sampling of the geologic provinces of interest. Recording sites are identified by the letters “sa” (southern Africa) and a number, e.g. sa70 (Figure 3).

The seismic experiment was conducted in such a way that data were recorded at some sites for one year only and the equipment was then transferred to the other sites. Stations along the central axis of the array were left in place to record for the whole two-year period of the experiment. The recording duration at each site is indicated by a colour-coded circle in Figure 3. In Zimbabwe data were recorded at nine sites, four for one year (sa75, sa77, sa79 and sa80) and five for two years (sa72, sa73, sa74, sa76 and sa78).

The seismographs used in the Southern Africa Seismic Experiment were digital, broadband systems with a flat velocity response over a frequency bandwidth of 0.008 to 10 Hz, where the high frequency cutoff (the Nyquist frequency) is controlled by a sampling rate of 20 samples per second (20 sps). Most of the equipment used were sourced from PASSCAL Instrument Centre (United States of America) with additional instrumentation from the Carnegie Institution of Washington (United States of America).

Receiver functions

Teleseismic P-waves incident upon a seismic discontinuity below a recording station produce P-to-S wave conversions at boundaries with significant S-wave velocity contrasts as well as multiple reverberations, particularly in the shallower layers. While the P-to-S wave conversions have much stronger amplitudes on the radial component than on the vertical component, they are dwarfed by the large amplitude direct-arriving P-waves. Teleseismic P-waves (with

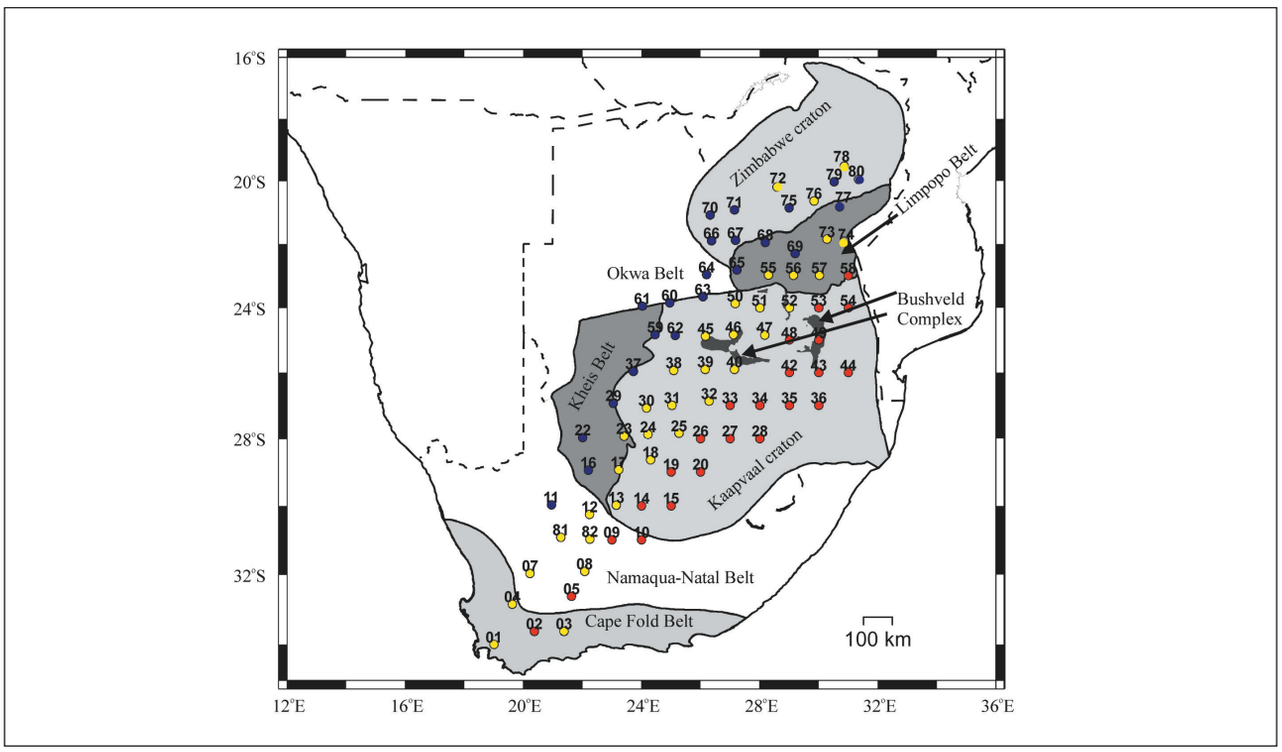

Figure 3. *Station array for the Southern Africa Seismic Experiment. Blue circles: stations that recorded data in the first year only. Yellow circles: stations that recorded data for the whole two-year period. Red circles: stations that recorded data in the second year only.*

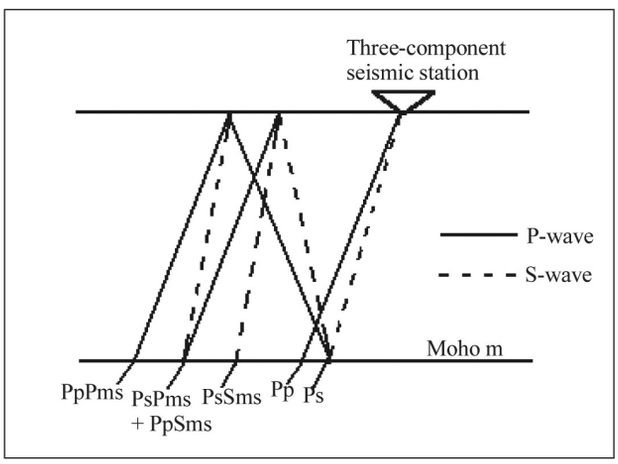

Figure 4. *Arrivals generated by a Moho discontinuity (after Ammon, 1991). Lower case indicates up-going waves and upper case down-going waves between the Moho and the surface, e.g. PpPms means a wave that arrives at the Moho as a P-wave, refracts to the surface as a P-wave, reflects from the surface as a P-wave and converts upon reflection at the Moho to an S-wave which then travels to the surface to be recorded at the station.*

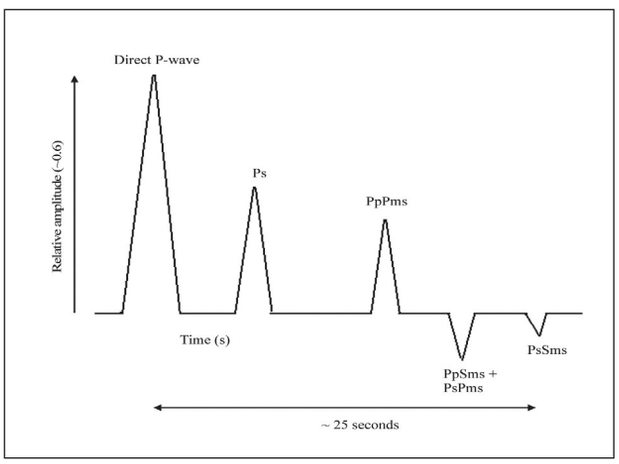

Figure 5. *Schematic radial receiver function (after Ammon, 1991). Phase notation here is as given in caption for Figure 4.*

epicentral distances >30°) are essentially the only phases recorded owing to the steep angles of the incident arrivals (Ammon, 1991). By deconvolving the vertical signal from the radial and transverse components, the complicating effects of source time history, near source structure and instrument response can be removed, leaving a signal composed primarily of conversions and reverberations of the P-to-S wave type (Langston, 1979) below the seismic station. This deconvolved radial component signal is termed the source equalised record or receiver function (Langston, 1979).

By the process of deconvolution, all of the P-wave energy that is coherent on both the vertical and radial components (in other words, all energy that arrives at the station as P-wave energy, including the first arrival and the entire P-wave coda) is compressed in the first "direct arrival" (or coherence peak) at the start of the deconvolved radial trace (Assumpcaõ et al., 2002). The signals that remain on the source equalised trace are

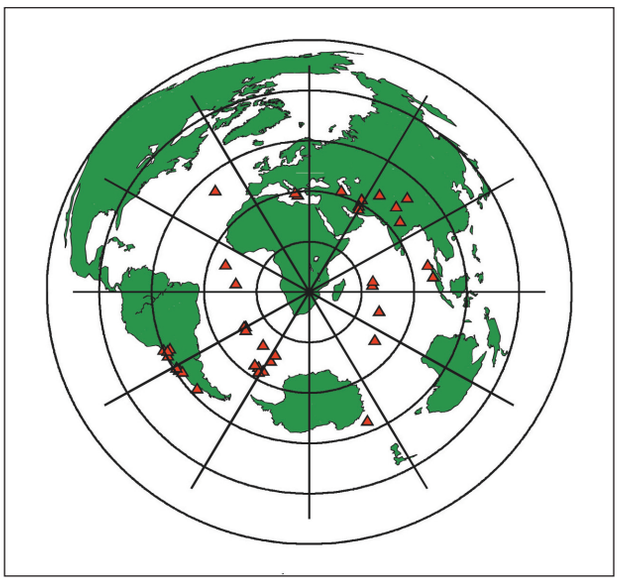

Figure 6. *Location map of the teleseismic events used in the receiver function analysis. Red triangles indicate the events' epicentres. Concentric circles represent epicentral distances from centre of array at 30° intervals and radial lines represent backazimuthback azimuths at 30° intervals from north.*

primarily P-to-S conversions. Receiver functions are thus time series waveforms constructed from three-component seismograms by deconvolving the vertical from the radial component of motion to isolate the converted S-wave phases within the coda of the P-waves (e.g. Langston, 1979; Owens et al., 1984; 1987; Ammon et al., 1990; Paulssen et al., 1993; Zandt et al., 1995; Last et al., 1997). The computing of deconvolved, or source equalised, records requires matched three-component seismograms (Ammon, 1991). An illustration of conversions produced by a sharp horizontal velocity discontinuity, such as the Moho, is depicted in Figure 4 (for rays) and Figure 5 (for the radial receiver function).

Since receiver function studies involve the analysis of teleseismic waveforms, this means the event generating the waves must be sufficiently distant from the recording station that body waves arrive at the station at close to vertical incidence. Typical teleseismic epicentral distances range from 27° to 95°. Events at distances less than 27° are complicated by travel time triplications from the upper mantle transition zone and are thus avoided in receiver function studies. Events beyond 95° are not used as they have complicated waveforms and limited frequency content due to diffraction at the core-mantle boundary.

All the teleseismic events used in the receiver function analysis in this paper are listed in Table 1 in chronological order, while Figure 6 shows the events' epicentres. The availability of a data set collected over a period of two years, allowed for selection of a high quality dataset. For this study we analysed 42 teleseismic events occurring at epicentral distances between 34° and 85° with a body wave magnitude, m_b ≥5.4. Raw data were processed into records that began five seconds prior to the direct P-wave arrival and continued for 30 seconds after (Ammon et al., 1990), a time window that contains all of the converted and reverberation phases from the Moho. Setting the onset of the time

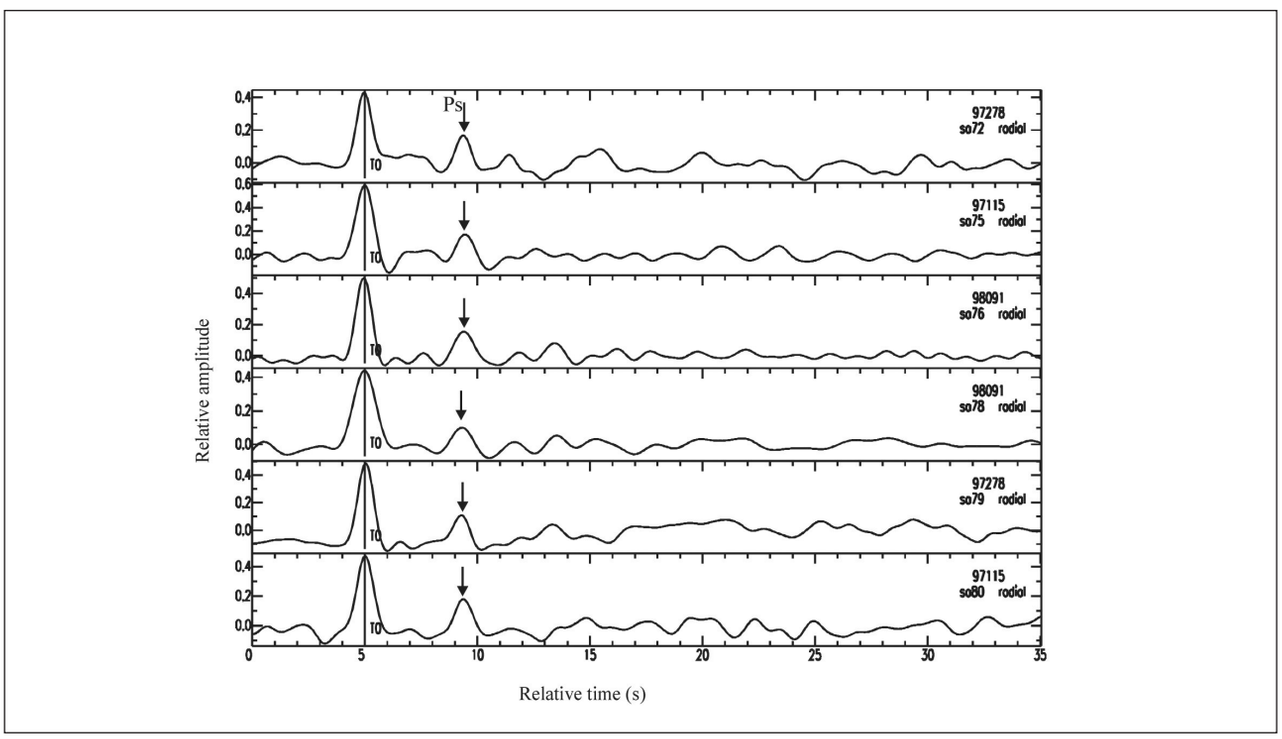

Figure 7. *Typical radial receiver functions for all the six stations on undisturbed Zimbabwe Craton.*

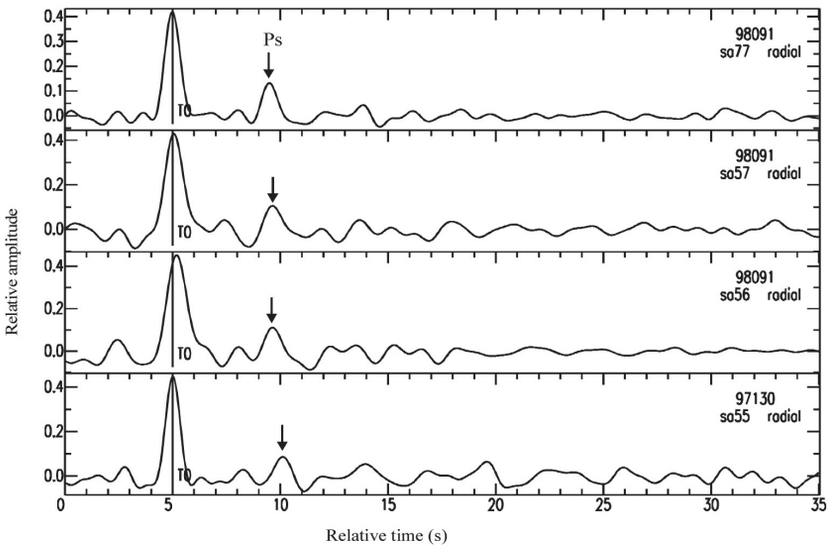

Figure 8. *Typical radial receiver functions for stations on the marginal zones of the Limpopo Belt.*

window five seconds prior to the direct P-wave arrival provided a check on the pre-signal noise level. This helped in determining whether an event was suitable for further processing.

Radial and tangential receiver functions, as well as the averaging function, were calculated for each of the 42 events at each station. The following parameters were used: values of trough fillers in the ranges of 0.0003, 0.003 and 0.03, and a Gaussian scale of 3 s^{-1} and occasionally 2 s^{-1}. Appropriate values for trough filler and Gaussian scale were arrived at by trial and error after taking into consideration the noise level introduced into the data from processing as well as the smoothness of the averaging function.

Results

Examples of the radial receiver functions for stations of the Zimbabwe array and other surrounding stations for some events recorded by the array are shown in Figures 7 to 9. Although stations sa66, 67, 70, and 71 appear on the station map (Figure 3) on the Zimbabwe craton, they are in the southwestern region of the craton strongly

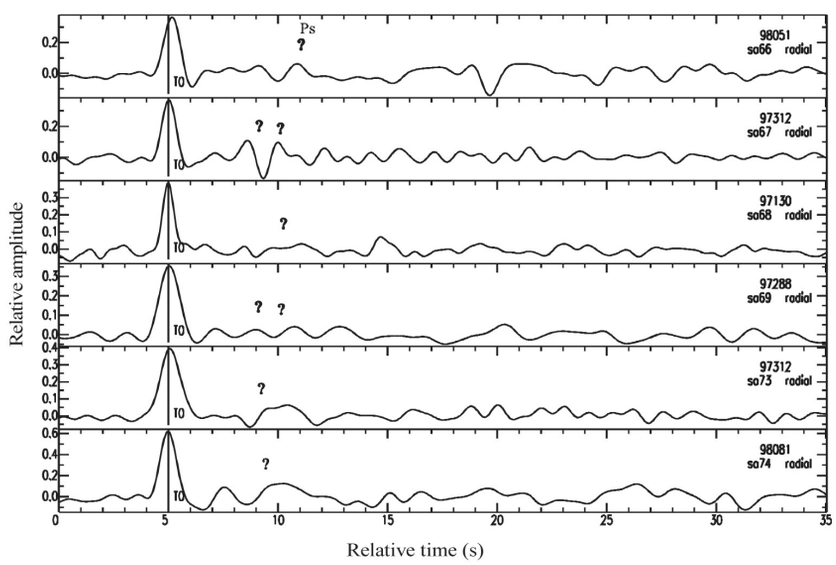

Figure 9. *Typical radial receiver functions for stations on the CZ of the Limpopo Belt.*

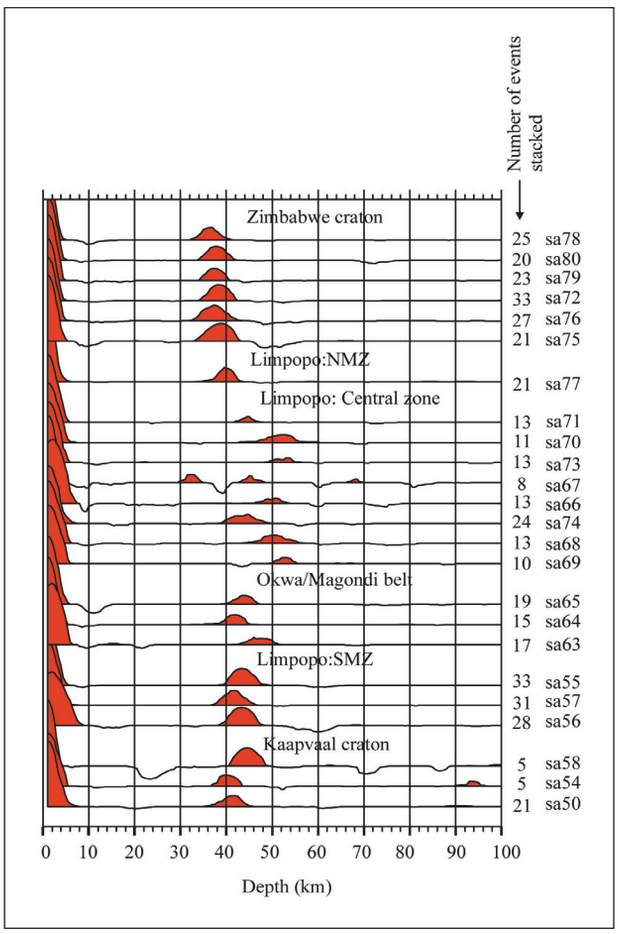

Figure 10. *Phasing depth images for all stations in the study area for a Poisson's ratio of 0.25 and a crustal thickness of 39 km.*

affected by the ~2.2 to ~2.0 Ga events and they are thus included in the CZ in this discussion.

Figure 7 shows typical traces for the six stations located on the undisrupted Zimbabwe craton. The Moho Ps conversion is at about 9.3 seconds on the scale of the plots, where the coherence peak corresponding to the direct P-wave is at 5 seconds. The Moho converted phases have similar lapse times (Ps-P) on all traces, suggesting an almost uniform depth to the Moho under these stations (Figure 7). In general, the receiver functions recorded at stations on the undisturbed Zimbabwe craton exhibit sharp, large amplitude Ps conversions, suggesting a sharp Moho beneath the craton.

Typical receiver functions for stations on the Southern Marginal Zone (sa55, sa56 and sa57) and one on the Northern Marginal Zone (sa77) are shown in Figure 8. These traces also have sharp and large amplitude Moho Ps conversion arrivals, similar to those for the undisturbed craton, again suggesting a sharp Moho discontinuity. One difference between the SMZ and NMZ traces is that Moho Ps arrivals at the SMZ stations arrive slightly later relative to the NMZ station, which suggests that the Moho under the SMZ is deeper than that beneath the NMZ, if both terrains have a similar velocity-depth structure.

Figure 9 shows a representative set of receiver functions for stations in the CZ of the Limpopo Belt. These show quite a different result compared to those on the undisturbed Zimbabwe Craton, with no clear Moho Ps conversion visible in the records. Some traces have a very broad Moho Ps conversion e.g. sa74, whilst others show two peaks between 4 and 6 seconds after the direct P arrival e.g. sa66, sa67 and sa69. This could be due to a complex Moho discontinuity structure under the stations or a result of a gradational Moho discontinuity.

Before analysing receiver functions to obtain structure, data are usually stacked to improve the signal to noise ratio. The stacking process is normally done for data from similar regions based on both distance and back azimuth, as arrival times show a dependence on ray parameter. However, data from different distances (hence with different ray parameters) can be stacked after correcting for moveout, to get an average structure in which effects such as Moho dip are ignored.

Moveout is defined as the functional dependence of arrival times on ray parameter relative to a reference phase (Gurrola *et al.*, 1994). The moveout time, T_{move} is derived using the equation:

$$T_{move} = h\left[\left(V_s^{-2} - p^2\right)^{\frac{1}{2}} - \left(V_p^{-2} - p^2\right)^{\frac{1}{2}}\right] \qquad (1)$$

where V_p and V_s are average P- and S-wave velocities respectively, p is the ray parameter and h is the depth to the discontinuity causing the P-to-S wave conversion. Taking $V_p/V_s = r$, reduces Equation 1 to,

$$T_{move} = \frac{h}{V_s}\left[\left(1 - p^2V_s^2\right)^{\frac{1}{2}} - \left(\frac{1}{r^2} - p^2V_s^2\right)^{\frac{1}{2}}\right] \qquad (2)$$

Equation 2 was used in this study to calculate moveout times. To determine the depth to the Moho under the stations, phasing analysis of the entire data set was performed (e.g. Gurrola *et al.*, 1994; Dueker and Sheehan, 1997, 1998). The receiver functions were binned by station and summed using N-th root stacking (Kanasewich, 1981) for a range of discontinuity depths from 1 km to 101 km at 0.5 km steps along trial Ps moveout curves. For a true Ps arrival the amplitude of the arrival is maximised when the correct phasing depth (i.e. moveout curve) is used. The resulting receiver functions are therefore stacks produced by N-th root stacking of M receiver functions with different ray parameters along moveout curves. The discontinuity structure below each station is hence shown as a spatial or phasing depth spike.

N-th root stacking has the advantage of increasing the signal to noise ratio as the resulting amplitude includes a coherency term, which has an effect of efficiently suppressing non-coherent phases on the receiver functions. This coherency term is absent in

Table 1. List of teleseismic events used in the receiver function analysis. YYDDD is the Julian day, M_s = surface wave amplitude, m_b = body wave magnitude, Δ = epicentral distance and BAZ = back azimuth.

Event YYDDD	Origin Time	Latitude (degree)	Longitude (degree)	Depth (km)	m_b	M_s	Δ (degree)	BAZ (degree)
97115	09 11	-48.342	-10.040	10.0	5.4	5.8	34.555	222.5
97130	07 57	33.825	59.809	10.0	6.4	7.3	68.904	30.6
97133	14 13	36.411	70.945	196.0	6.1	0.0	76.472	36.6
97141	22 51	23.083	80.041	36.0	6.0	5.6	72.836	52.2
97153	21 24	-57.776	-25.466	33.0	5.9	5.8	46.735	214.6
97185	09 54	-58.055	-11.180	10.0	5.5	5.2	40.076	209.2
97200	12 22	-29.281	-71.684	26.0	5.8	5.5	82.609	241.0
97201	10 14	-22.982	-66.301	256.0	5.7	0.0	81.009	248.9
97232	13 51	-41.715	80.134	10.0	5.6	6.4	47.048	123.0
97261	18 19	-60.722	-24.479	33.0	5.4	5.1	47.312	210.6
97268	14 20	-13.761	66.248	10.0	5.4	5.7	40.642	79.5
97278	18 04	-59.739	-29.198	274.0	6.0	0.0	49.194	212.9
97286	13 39	36.379	22.071	24.0	6.2	6.6	63.092	357.3
97288	04 28	-30.809	-71.251	48.0	5.5	0.0	81.594	239.8
97307	19 17	-30.744	-71.224	9.0	6.2	5.6	81.602	239.9
97312	10 02	35.069	87.325	33.0	6.2	7.9	85.297	46.8
97322	13 07	37.570	20.656	33.0	5.9	6.4	64.380	356.2
97361	20 11	-55.783	-4.218	10.0	5.4	5.3	35.672	208.2
98003	06 10	-35.474	-16.191	10.0	5.4	5.9	36.029	246.1
98012	10 14	-30.985	-71.410	35.0	5.8	6.2	81.638	239.6
98030	12 16	-23.913	-70.207	42.0	6.3	6.3	83.825	246.4
98051	12 18	36.479	71.086	23.6	5.8	5.7	76.599	36.6
98073	19 40	30.154	57.605	9.0	5.9	6.9	64.813	31.0
98081	01 08	-11.430	66.245	10.0	5.4	6.1	41.680	76.3
98084	03 12	-62.877	149.527	10.0	6.6	8.0	80.238	157.5
98088	07 14	-0.239	-17.932	10.0	5.5	5.6	49.085	295.6
98091	17 56	-0.544	99.261	56.0	6.2	6.9	75.724	83.2
98091	22 42	-40.316	-74.874	9.0	6.2	6.0	79.997	229.1
98115	06 07	-35.266	-17.326	10.0	5.5	5.5	36.951	246.5
98169	04 17	-11.572	-13.894	10.0	5.4	6.1	39.618	285.1
98175	10 44	-37.295	-17.391	10.0	5.7	5.8	37.083	243.1
98190	05 19	38.650	-28.626	10.0	5.7	6.0	82.336	320.5
98190	14 19	38.717	48.507	26.0	5.9	0.0	68.961	19.5
98210	07 14	-32.312	-71.286	51.0	6.3	0.0	80.958	238.5
98241	08 30	-55.737	-27.045	33.0	5.6	5.6	46.955	217.6
98246	17 37	-29.450	-71.715	27.0	6.2	6.6	82.557	240.9
99024	08 00	-26.463	74.476	10.0	6.0	6.3	43.942	101.0
99035	19 28	4.033	95.283	56.0	5.8	5.4	74.391	77.1
99048	21 58	-21.143	-70.040	33.0	5.6	5.1	84.928	249.0
99061	17 45	-22.717	-68.503	111.0	5.8	0.0	82.962	248.2
99063	05 38	28.343	57.147	33.0	6.2	6.5	63.093	31.8
99087	19 05	30.512	70.403	15.0	6.4	6.6	77.267	46.0

linear stacking. In this study, N = 4 was found to be the optimal value.

Since the stacking programme requires a velocity model to calculate the moveout, a total of 15 SAF starting models were tried in this study, where SAF stands for southern Africa. The starting models were derived from the IASPEI91 model (Kennett and Engdahl, 1991). For a particular crustal Poisson's ratio, models with the following average crustal thickness were used: 34 km, 39 km and 45 km. The crustal Poisson's ratios used ranged from 0.24 to 0.28, values that fall within the normal range for common rock types of 0.20 to 0.35 (Zandt and Ammon, 1995). However, only those results obtained for models with a crustal thickness of 39 km with varying Poisson's ratio are discussed since it was observed that changing the crustal thickness in the model for a particular Poisson's ratio did not have a significant effect on the results. The calculated Moho depths changed at most by 1 km after varying the crustal thickness from 34 km to 45 km in the models.

All the phasing depth images for the study area obtained using the SAF model with a Poisson's ratio of

0.25 and a crustal thickness of 39 km are shown in Figure 10, organised by geological regions. The first zero-depth peak corresponds to the coherence peak of P-wave arrivals, with subsequent peaks relating to discontinuities at depth. Moho depths were picked at the highest amplitude of the peaks, and for most cases these points coincided with the centre of the peaks. The corresponding Moho depths obtained for each station for each model are tabulated in Table 2. The data for the Poisson's ratio of 0.25 were used to produce Figure 11(a) a 3-D structure map of the Moho relief beneath the study area and Figure 11(b), a contour map of crustal thickness beneath the study area. The additional data used to plot the area south of the SMZ were adopted from Nguuri *et al.* (2001).

The typical estimated uncertainty in the calculated Moho depth is ± 2 km. This value was obtained by assuming a 3% error in both P- and S-wave velocities used in the velocity model and a 10% combined error in the ray parameter and phase arrival time determinations. Poorly defined Ps conversions can add substantial additional uncertainty to Moho depth.

Zimbabwe craton

All stations on the craton have sharp, large amplitude Ps converted signals from the Moho discontinuity (Figure 10). The results suggest an unlayered crustal structure with a sharp Moho discontinuity at a minimum depth of 33 km for a Poisson's ratio of 0.28 and a maximum depth of 40 km for a Poisson's ratio of 0.24. Representing the average crust under the stations by a Poisson solid, i.e. σ = 0.25, the depths to the Moho tightly cluster between 36.5 km and 39 km. This would translate into a fairly flat Moho discontinuity structure in the craton below the area covered by the stations.

Limpopo Belt

The single station located in the NMZ of the Limpopo Belt, sa77, has a receiver function image typical of the adjacent Zimbabwe craton (Figure 10). The Ps conversion from the Moho is sharp and large amplitude, giving a calculated Moho discontinuity at a minimum depth of 36 km for a Poisson's ratio of 0.28 and a maximum depth of 41 km for a Poisson's ratio of 0.24. Receiver function images for the SMZ are also sharp and of large amplitude, giving a Moho discontinuity at depths between 38 km and 45 km for the range of Poisson's ratios used. These depths are consistent with results for the northern edge of the Kaapvaal Craton (Nguuri *et al.*, 2001). Comparison of the Moho depths for the two marginal zones shows that the two terrains are not necessarily mirror images of each other. Rocks in these terrains might be similar but the Moho discontinuity seems deeper under the SMZ than under the NMZ for the same Poisson's ratio.

Images for stations in the CZ display complex structure below this terrain, with no clear pattern among the stations, in agreement with results of Nguuri *et al.*

Table 2. Estimated Moho depths for the study area from models with various Poisson's ratios and a crustal thickness of 39 km.

Station	Moho depth (km) (σ = 0.24)	Moho depth (km) (σ = 0.25)	Moho depth (km) (σ = 0.26)	Moho depth (km) (σ = 0.27)	Moho depth (km) (σ = 0.28)	Location
sa78	37.5	36.5	35.0	34.0	33.0	Zimbabwe Craton (ZC)
sa80	39.0	38.0	36.5	35.5	34.0	
sa79	38.5	37.5	36.0	35.0	33.5	
sa72	40.0	38.5	37.0	36.0	34.5	
sa76	38.5	37.5	35.5	34.5	33.5	
sa75	40.0	39.0	37.5	36.5	35.0	
sa77	41.0	39.5	38.0	37.0	36.0	Northern Marginal Zone (NMZ)
sa70	55.0	52.5	51.0	49.5	47.0	Limpopo: Central Zone (CZ)
sa71	46.5	44.5	43.0	41.5	40.0	
sa73	55.0	53.0	51.0	49.5	47.5	
sa74	46.5	44.5	43.0	41.5	39.5	
sa66	52.5	51.0	49.0	46.0	45.0	
sa67	47.0; 33.0	45.0; 32.0	43.5; 31.0	42.0; 30.0	40.5; 29.0	
sa68	52.5	50.5	48.5	47.0	45.5	
sa69	55.0	52.5	50.5	49.0	47.0	
sa65	45.5	44.0	42.0	41.0	39.0	Okwa/Magondi Belt
sa64	43.5	42.0	40.0	39.0	37.5	
sa63	48.0	47.0	44.0	44.5	41.0	
sa55	45.0	43.5	41.5	40.5	38.5	Southern Marginal Zone (SMZ)
sa57	43.0	41.5	39.5	38.5	37.0	
sa56	45.0	43.5	41.5	40.5	38.5	
sa58	46.5	44.5	43.0	41.5	39.5	Kaapvaal Craton
sa54	41.0	40.0	38.0	37.0	35.5	
sa50	43.0	41.5	39.5	38.5	37.0	

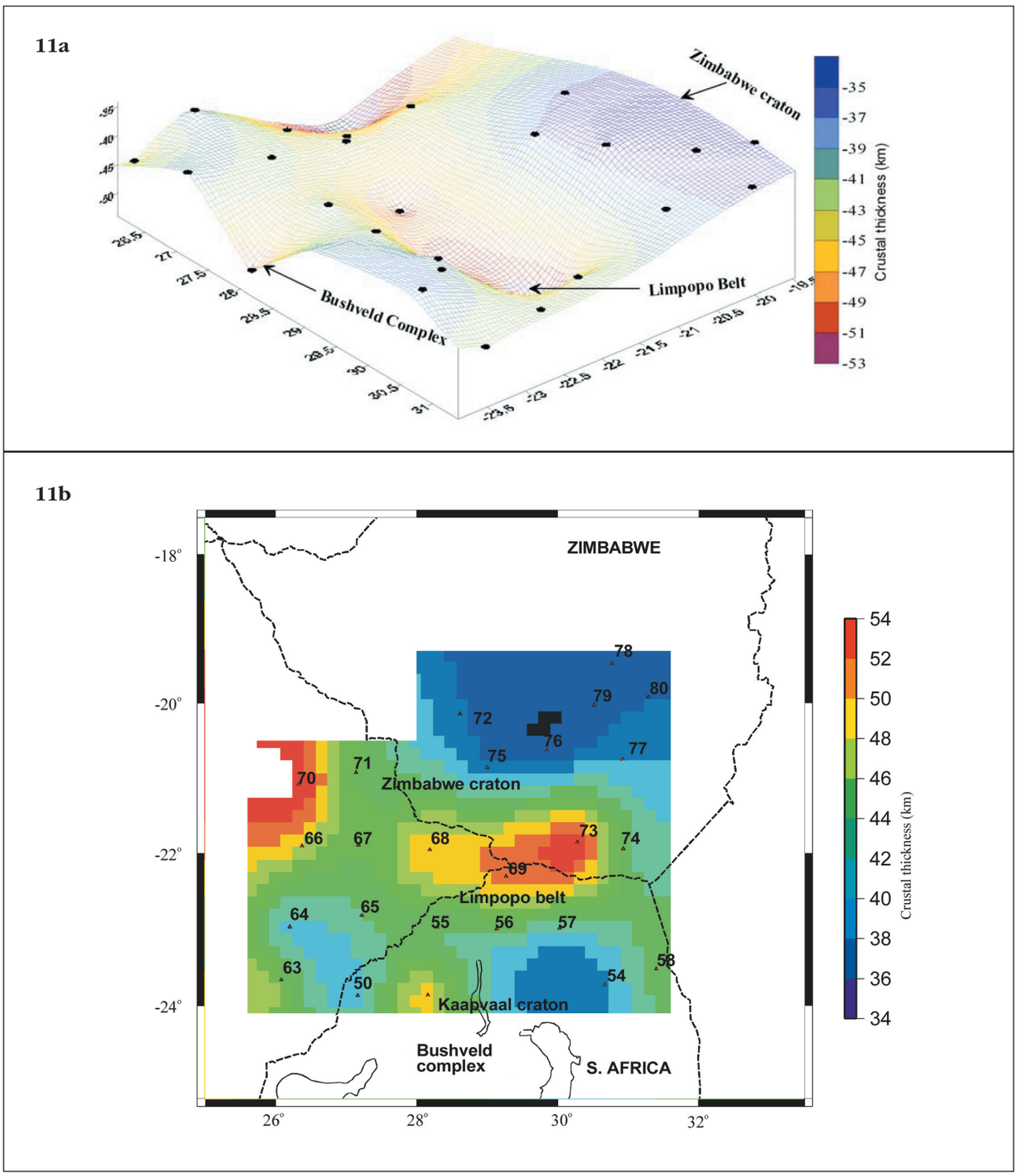

Figure 11. *(**a**). Average 3-D map of the Moho discontinuity under the study area for a Poisson's ratio of 0.25 and a crustal thickness of 39 km. Black dots indicate station locations at the surface (see Figure 3). Data for the Bushveld Complex is from Nguuri et al. (2001). (**b**). Contour map of crustal thickness beneath the study area for a Poisson's ratio of 0.25 and a crustal thickness of 39 km.*

(2001). For some stations to the west of the belt in Botswana, e.g. sa67, the identification of the Moho Ps conversion is ambiguous because of the presence of two almost equal signals indicating discontinuities at average depths of 32 km and 45 km for a Poisson's ratio of 0.25. For some stations, e.g. sa74, there is a very broad discontinuity at an average depth of 43.5 km, while the adjacent station, sa73 has a very small peak indicating a discontinuity at an average depth of 51 km (Figure 10). However, except for sa67 these results indicate a Moho that varies in depth between about 40 km and 52 km. This implies that the crust of the Limpopo Belt is thicker than that of the adjacent marginal zones and the Zimbabwe Craton.

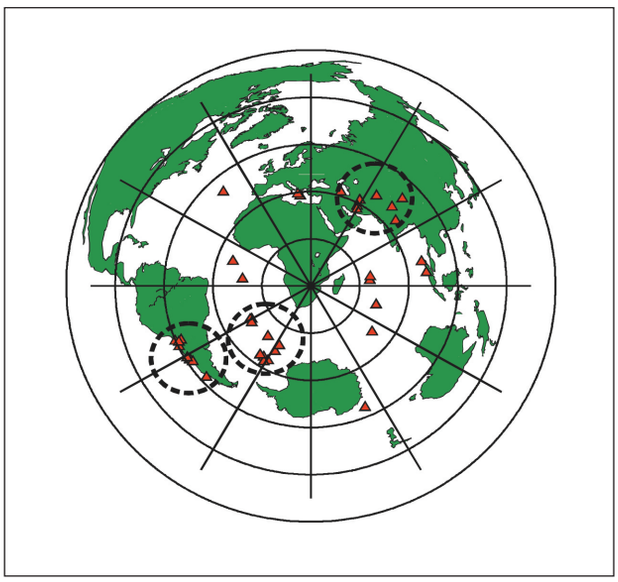

Figure 12. *Map showing epicentres of all the events used in this study and the corresponding event groups as indicated by broken circles.*

Kaapvaal Craton and Okwa/Magondi Belt

Results for stations sa58, sa54 and sa50 on the northern edge of the Kaapvaal Craton reveal a relatively sharp Moho discontinuity at depths between 40 and 44 km for a Poisson's ratio of 0.25. These values agree with those found for the rest of the Kaapvaal craton by Nguuri et al., (2001).

The three stations on the Okwa/Magondi Belt, sa65, sa64 and sa63 have sharp but not large amplitude Ps conversions from the Moho (Figure 10). The results suggest the Moho to be at depths between 42 and 47 km for a Poisson's ratio of 0.25.

Structural variation with azimuth

Since stacking events from different directions smoothes out any effects of 3-D geology, it is necessary to organise events into groups based on both back azimuth and epicentral distance before stacking. This facilitates study of the variation in the response with direction or back azimuth as waves approaching a seismic station from different directions may sample very different structures, i.e. structure may vary with azimuth. This variation can be due to dipping of the Moho, anisotropy or lateral inhomogeneities (Gurrola *et al.*, 1994; Savage, 1999). For this study, events that occurred within to 40° of each other for both back azimuth and epicentral distance were taken to be originating from the same point and the corresponding receiver functions were therefore stacked. Figure 12 shows event locations on the world map and hence the main regions from which events were taken, the data of which were used to produce receiver functions stacked by azimuth. Three main regions were identified, around Iran (northeast), the Andes and South Sandwich Islands (southwest). The Andes and Sandwich Islands events were stacked together.

In general, results for stations on the Zimbabwe Craton for events from southwestern regions, shown in Figure 13, do not show a marked difference from those of events from the northeastern region, Figure 14. This implies that structure under all stations on the Zimbabwe Craton is largely independent of back azimuth. Hence the Moho discontinuity under the six stations on the Zimbabwe Craton does not vary much with azimuth, an indication of a fairly flat and simple Moho discontinuity structure. This is also true for the four marginal zone stations, whose phasing depth images show no structural variation with back azimuth.

Results for the Limpopo Belt do show a structural azimuthal dependence for some stations, as phasing depth images produced for events from the southwest regions, Figure 13, show a marked difference for events from the northeast region, Figure 14. For stations sa66 and sa67 events from the northeast are suggesting two discontinuities at depths of 32 to 35 km and another one at 45 to 51 km. This is in contrast to the southwest events, which sample only the 32 to 35 km discontinuity under sa67 and only the 45 to 51 km under sa66. Under sa69 the single discontinuity around 53 km suggested by events from the southwest is not sampled by events

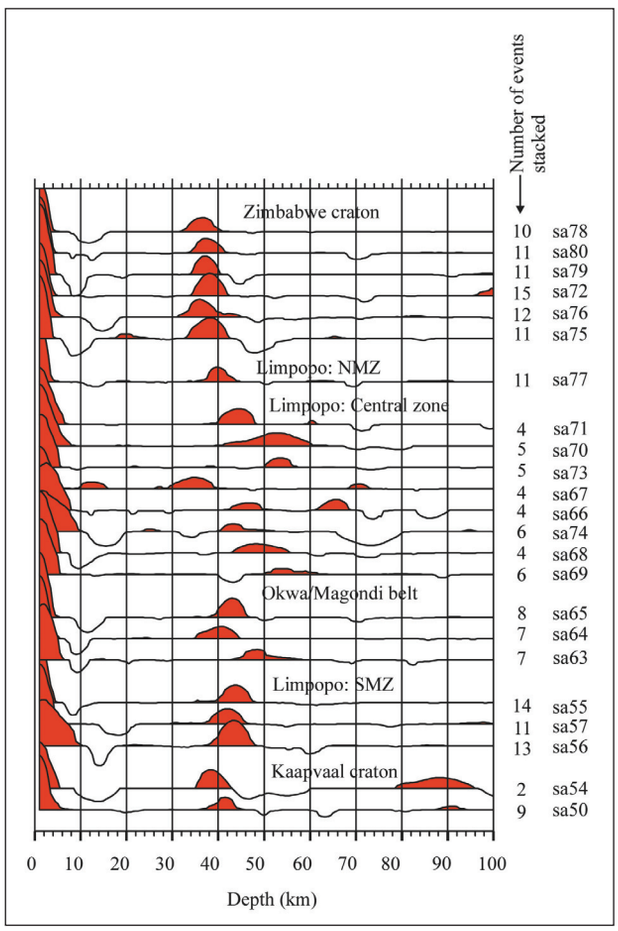

Figure 13. *Phasing depth images for events from the southwest region.*

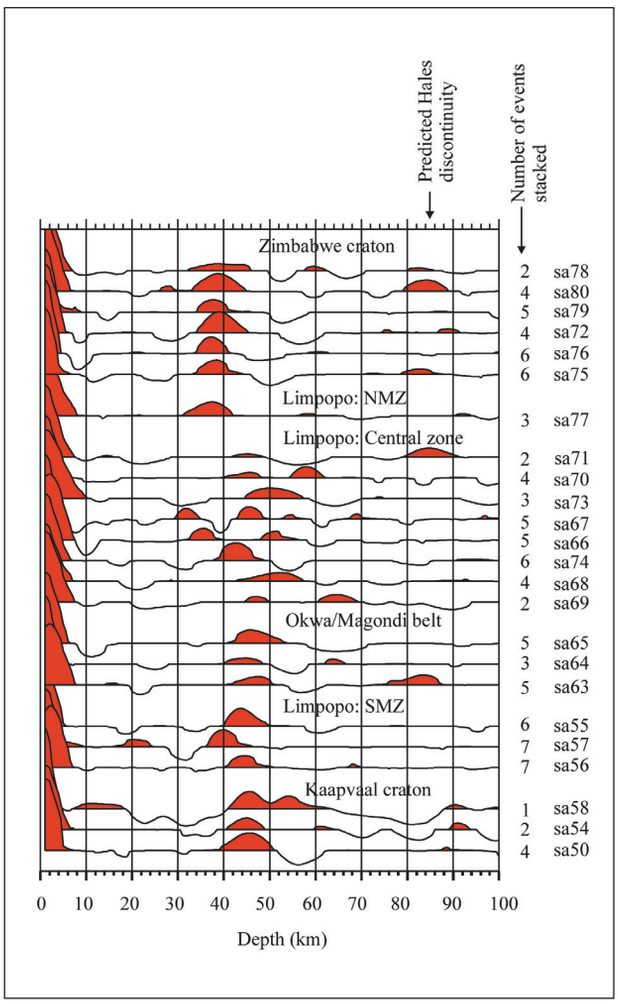

Figure 14. *Phasing depth images for events from the northeast region.*

from the northeast, which suggest two discontinuities, one at around 47 km and another at 65 km. From these results, it is not apparent in which direction the Moho under the stations in the CZ is dipping. Hence the pattern displayed by the phasing images could simply be a manifestation of the complexity of the Moho discontinuity structure in the CZ.

Events from the northeast region also show a strong discontinuity beneath some stations (e.g. sa80, sa71, sa63) at a depth of between 80 and 90 km. While the phases could be conversions from the Hales discontinuity (Hales, 1969), thought to be due to the petrologic transition from spinel to garnet peridotite, the results are ambiguous because crustal reverberations are also predicted over that depth interval.

Poisson's ratio estimates

Poisson's ratio is defined as the ratio of the lateral strain to the longitudinal strain when a uniaxial force is applied to an object. It is an important parameter in seismology for distinguishing rock compositions in the crust, e.g. mafic versus intermediate versus silicic. Mafic and ultramafic rocks tend to have higher Poisson's ratios

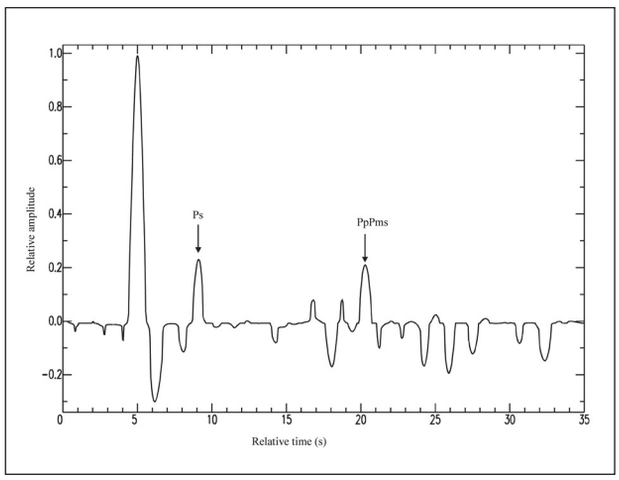

Figure 15. *Receiver function stack for sa78 for four events from the Andes region.*

(σ >0.26) and silicic rocks tend to have lower ratios (σ <0.26) (Zandt and Ammon, 1995). In this study, Poisson's ratio estimates under each station were calculated based on the method of Niu and James (2002), using Ps and PpPms phase travel times (see Figure 15).

For each station, receiver functions were first grouped by back azimuth and distance and then each group stacked. An N-th root stacking method with N = 4 was used to increase the signal to noise ratio. As an example, Figure 15 shows the result of stacking four receiver functions for events from the Andes region for station sa78 on the Zimbabwe Craton.

The travel time differences or lapse times between the coherent peak and each of Ps and PpPms phases can be expressed as follows:

$$T_{Ps} = h\left(\frac{\cos\beta}{V_s} - \frac{\cos\alpha}{V_p}\right) \quad (3)$$

$$T_{PpPms} = h\left(\frac{\cos\beta}{V_s} + \frac{\cos\alpha}{V_p}\right) \quad (4)$$

where α and β are angles of incidence of P- and P-to-S converted waves, respectively. Equations 3 and 4 can be combined to get:

$$\frac{V_p}{V_s} = \frac{T_{Ps} + T_{PpPms}}{T_{PpPms} - T_{Ps}} \frac{\cos\alpha}{\cos\beta} \quad (5)$$

Equation 5 gives the relationship between the ratio of P- and S-wave velocities to the Ps and PpPms lapse time and the incident angles of P- and P- to S- converted waves. The angles α and β were calculated by ray tracing using the IASPEI91 model. Poisson's ratios, σ were then calculated using the equation,

$$\sigma = \frac{\left(\frac{V_p}{V_s}\right)^2 - 2}{2\left(\frac{V_p}{V_s}\right)^2 - 2} \quad (6)$$

Results obtained for the three event regions (Figure 12) where the PpPms phase was identifiable are shown in Table 3. The trend is that undisturbed cratonic areas have lower Poisson's ratios (0.240 to 0.262) while off-cratonic areas have higher values (0.251 to 0.293). This suggests on average a crustal composition of silicic to intermediate composition under the undisturbed craton, and crust of more mafic composition under the Limpopo Belt and the Okwa/Magondi terrains. This agrees with observations made by Durrheim and Mooney (1991) that disturbed cratonic areas or younger terrains tend to have more mafic lower crusts than undisturbed cratonic areas.

The calculated standard error in the mean (SEM) for the Poisson's ratios are: ± 0.002 for the Zimbabwe Craton, ± 0.005 for the CZ and ± 0.004 for the SMZ. It was not possible to calculate the SEM for the NMZ, Okwa/Magondi belt and Kaapvaal Craton as these three regions each had less than four Poisson's ratio estimates.

Discussion and conclusion

Results from the analysis of receiver functions revealed that there are significant differences between the character of the Moho discontinuity under the Zimbabwe Craton and under the Limpopo Belt, irrespective of the value of the Poisson's ratio used. In this discussion those regions of the craton affected by post stabilisation events (<2.5 Ga, see Section 2.2.1) are referred to as disturbed craton.

Results for the undisturbed parts of the Zimbabwe Craton (Table 2 and Figures 11(a) and (b)) show Moho depths ranging between 36.5 km (under sa78) to 39 km (under sa75) for a Poisson's ratio of 0.25. P-to-S wave conversions indicate that the Moho is a sharp and relatively simple structure beneath the craton. Our results show no evidence of any major mid-crustal discontinuities beneath the stations on the craton. This would suggest that the crust under the southern part of the Zimbabwe Craton is not distinctly layered. Moreover, the results show no evidence of high reflectivity layering in the lower crust, although fine-scale layering could have escaped detection in the receiver function method used here. In the presence of distinct layering, the effect on receiver functions would be a broadened Ps phase.

Results from stations on the disturbed parts of the craton in the south-westernmost part of the Zimbabwe Craton (in Botswana), notably sa70 and sa71, reveal Moho Ps signatures very different from those for the undisturbed parts of the craton. These two stations reveal a deeper and more diffuse Moho discontinuity at depths of 52.5 and 44.5 km respectively. This observation might be an expression of the 2.0 Ga event that affected the Limpopo Belt and this region in eastern Botswana as suggested by McCourt and

Table 3. Estimates of Poisson's ratios under the stations: σ_1 are calculated from Iran events, σ_2 from Sandwich Islands events and σ_3 from Andes events. Numbers in parentheses (n) indicate the number of events averaged for each value.

Station	σ_1		σ_2		σ_3		Location
sa78	–		0.250	(3)	–		Zimbabwe Craton (ZC)
sa80	0.253	(4)	–		0.250	(5)	
sa79	0.249	(5)	–		0.262	(6)	
sa72	–		0.245	(4)	0.249	(10)	
sa76	0.249	(6)	0.244	(6)	0.241	(8)	
sa75	0.248	(6)	0.240	(4)	0.248	(7)	
sa77	–		–		0.246	(7)	Northern Marginal Zone (NMZ)
sa71	0.276	(4)	0.268	(2)	–		Limpopo: Central Zone (CZ)
sa70	0.293	(5)	–		–		
sa73	–		0.274	(5)	–		
sa74	0.258	(6)	0.257	(4)	–		
sa66	0.284	(5)	–				
sa67	0.275	(5)	–		0.245	(4)	
sa68	–		–		0.291	(3)	
sa69	–		–		–		
sa65	–		0.253	(3)	0.262	(4)	Okwa/Magondi Belt
sa64	–		0.251	(3)	–		
sa63	–		–		–		
sa55	0.240	(5)	0.259	(5)	–		Southern Marginal Zone (SMZ)
sa57	–		0.256	(4)	0.264	(6)	
sa56	0.256	(7)	0.247	(4)	–		
sa58	–		–		–		Kaapvaal Craton
sa54	–		–		–		
sa50	–		0.251	(5)	0.258	(4)	

Armstrong (1998). They attribute the ~2.0 Ga event to the intrusion of Mahalapye granite and related granodiorite dykes, the Bulai granite of the CZ, the Razi suite of the NMZ and the Matok pluton of the SMZ, into their host granulites. It could also be due to igneous underplating possibly during the Karoo volcanism at circa 190 to 170 Ma (e.g. Eales et al., 1984; White and McKenzie, 1989). Although the locations on the geology map (Figure 3) of the two stations sa70 and sa71 are on the southern edge of the Zimbabwe craton, their receiver function signatures are very similar to those recorded by stations in the CZ. This suggests that these two stations are on disturbed craton or on the Limpopo Belt itself and not on undisturbed Zimbabwe Craton, as shown on the geology map.

While Moho Ps signatures from the Zimbabwe Craton are sharp and with large amplitude, signatures from the CZ of the Limpopo Belt are typically broad and with smaller amplitude. The CZ results reveal discontinuities of varying depth under the stations, ranging from about 40 km to 53 km (Figure 10).

One possible explanation for the series of discontinuities could be that the zone between 40 and 53 km is a broad Moho transitional zone, the remains of a crustal root from an ancestral collisional mountain belt. It is a puzzle that although the Moho beneath the CZ of the Limpopo Belt is deeper than that beneath the craton, the Belt has low topography relative to the adjacent cratons. It has been speculated on a geologic basis that during continent-to-continent collision ~ca. 2.7 Ga the crust of the CZ was thickened to as much as 70 km (Van Reenen et al., 1987). It then had 20 to 30 km of its upper crust exhumed, as indicated by relict kyanite inclusions in garnets, leaving high pressure metamorphic assemblages at the surface (Van Reenen et al., 1987). Hence, the present day CZ could be the remnant of a deep-rooted crustal block that did not fully rebound during denudation of the collisional belt mountains. This is not a unique circumstance. The reduced uplift in old mountain belts was first noted by Fischer (2002), who suggested that the loss of crustal root buoyancy in old roots (>100 Ma) was the result of metamorphic transformations that increase crustal root density. By this mechanism, the crustal root would remain in isostatic equilibrium even as the surface is reduced to low-lying topography by erosion. The notion of a dense root is consistent with gravity studies (e.g. Gwavava et al., 1992) that suggest the positive Bouguer anomaly in the Limpopo Belt may be due to a deep crustal source.

Another explanation would be that part of the dense root may even be related to possible underplating during Karoo volcanism. Such underplating would be consistent with the higher average Poisson's ratios that are observed in the crust of the CZ.

Results from this study and those from some previous studies differ significantly with regards to crustal thickness in the CZ of the Limpopo Belt. The present study shows that the shallowest depth to the Moho should be about 43 km and not 30 km as previously reported (e.g. Stuart and Zengeni, 1987). One possible explanation may be that this study and the other methods could be mapping differing regions of a broad Moho transition zone under the CZ. Although a weak peak is observed from a discontinuity at depths around 32 km under stations sa66 and sa67 (Figure 10), the stronger peaks from discontinuities at greater depths of 51 km (at sa66) and 44 km (at sa67), have been taken to be the Moho discontinuity under these stations. The weak peak around 32 km is closer to the Moho depth deduced by Gwavava et al. (1992) for a model with no underplating and by Stuart and Zengeni (1987). However, Gwavava et al. (1992) had also proposed a Moho depth at around 44 km for a model with underplating.

Results for the marginal zones of the Limpopo Belt also reveal significantly different Moho character with respect to that of the CZ. The single NMZ station, sa77, shows a sharp Moho discontinuity at depths of 36 to 41 km (for the range of Poisson's ratios used) typical of the adjacent Zimbabwe Craton. Stuart and Zengeni (1987) had proposed the presence of a 6 km step in the Moho from the craton into the NMZ, while Ridley (1992) had also expressed the view that the NMZ-Zimbabwe Craton contact is steep. Results from this study and those of Gwavava et al. (1992) do not support the presence of such a Moho step, a view echoed by Rollinson and Blenkinsop (1995) and Chiwara (2002) that this contact is gently dipping, as supported by evidence of surface geology. The three SMZ stations, sa55, sa56 and sa57 show a sharp Moho discontinuity at between 40 and 43 km depths, also typical of the adjacent Kaapvaal Craton.

Two inferences can be drawn from the above observations. Firstly, since Moho Ps signatures for the marginal zone stations have similar character to those on the adjacent cratons, i.e. sharp and large amplitude, this suggests that the Zimbabwe and Kaapvaal Cratons and the marginal zones have similar lower crustal structure. Secondly, although the two marginal zones both have sharp Moho discontinuities, the significant difference in their Moho depths seem to suggest that seismically the two zones are not mirror images of each other. This is based on the assumption, however, that the structure under station sa77 is representative of the entire NMZ structure. These limited results are consistent with geologic inferences that the NMZ and SMZ are overthrusts atop the Zimbabwe and Kaapvaal Cratons, respectively.

Estimates of Poisson's ratio that were determined in this study are averages for the whole crust, as the method used to calculate them does not permit calculation of the Poisson's ratios for the upper and lower crusts separately. The values obtained in this study from receiver function Ps and PpPmS phase arrival times range from about 0.24 to 0.26 for stations on the Zimbabwe and Kaapvaal Cratons, and 0.26 to 0.29 for stations in the Limpopo Belt. Although for some stations it was impossible to determine meaningful Poisson's

ratios, the overall trend is that cratonic areas have lower Poisson's ratios while disturbed areas have higher values.

These results suggest on average a crust of felsic to intermediate composition under the undisturbed craton, and of intermediate to mafic composition under the Limpopo Belt and the Okwa/Magondi terrains. The values obtained in this study are consistent with observations made by others (e.g. Durrheim and Mooney, 1991; Griffin and O'Reilly, 1987) that disturbed cratonic areas or younger terrains tend to have more mafic lower crusts than do undisturbed cratonic areas. Intermediate composition lower crust is also found beneath the Kaapvaal Craton, where very precise measurements by Niu and James (2002) show a lowermost crustal density of 2 860 kg m^{-3}. These observations are incompatible with assertions elsewhere in the literature that Poisson's ratio increases with the age of the crust, i.e. lower crust beneath cratons is more mafic as compared to younger terrains (e.g. Zandt and Ammon, 1995).

Acknowledgements

This research was supported by the NSF, Carnegie Institution of Washington, University of Zimbabwe and the Schlumberger Faculty for the Future Grant through the School of Geosciences at the University of Witswatersrand in South Africa. We would like to thank Tom Blenkinsop, Jan Kramers and a anonymous reviewer for their constructive reviews which improved this paper.

References

Ammon, C.J., Randall, G.E. and Zandt, G. (1990). On the nonuniqueness of receiver function inversion. *Journal of Geophysical Research*, **95**, 15303–15318.

Ammon, C.J. (1991). The isolation of receiver effects from teleseismic P waveforms. *Bulletin of the Seismological Society of America,* **81**, 2504–2510.

Armstrong, R. and Wilson, A.H. (2000). A SHRIMP U-Pb study of zircons from the layered sequence of the Great Dyke, Zimbabwe, and a granitoid anatectic dyke. *Earth and Planetary Science Letters*, **180**, 1–12.

Assumpcaõ, M., James, D.E and Snoke, J.A. (2002). Crustal thicknesses in SE Brazilian shield by receiver function analysis: implications for isostatic compensation. *Journal of Geophysical. Research*, **107**, X1-X14.

Bleeker, W. (2003). The late Archaean record: a puzzle in ca. 35 pieces. *Lithos,* **71**, 99–134.

Blenkinsop, T.G., Martin, A., Jelsma, H.A. and Vinyu, M.L. (1997). The Zimbabwe Craton. *In*: M.J. De Wit and L.D. Ashwal (Editors), Tectonic evolution of greenstone belts, *Oxford Monograph on Geology and Geophysics*, **35**, 567–580.

Brandl, G. and De Wit, M.J. (1997). The Kaapvaal Craton. *In*: M.J. De Wit and L.D. Ashwal (Editors), Tectonic evolution of greenstone belts, *Oxford University Monograph on Geology and Geophysics*, **35**, 581–607.

Chiwara, V. (2002). Late Archaean- Early Proterozoic Tectonics in the Northern Marginal Zone, Limpopo Belt, around Renco Mine, Implications for Au Mineralisation. *Unpublished M. Phil. tThesis , University of Zimbabwe, Harare, Zimbabwe*, 154pp.

Cox, K.G., Johnson, R.L., Monkman, L.J., Stillman, C.J., Vail, J.R. and Wood, D.N. (1965). The geology of the Nuanetsi igneous province. *Philosophical Transactions of the Royal Society of London*, **257**, 71–218.

Dueker, K.G. and Sheehan, A.F. (1997). Mantle discontinuity structure from midpoint stacks of converted P to S waves across the Yellowstone hotspot track. *Journal of Geophysical Research*, **102**, 8313–8327.

Dueker, K.G. and Sheehan, A.F. (1998). Mantle discontinuity structure beneath the Colorado Rocky Mountains and High Plains. *Journal of Geophysical Research*, **103**, 7153–7169.

Durrheim, R.J. and Mooney, W.D. (1991). Archaean and Proterozoic crustal evolution: evidence from crustal seismology. *Geology*, **19**, 606–609.

Durrheim, R.J., Barker, W.H. and Green, R.W.E. (1992). Seismic studies in the Limpopo Belt. *Precambrian Research*, **55**, 187–200.

Du Toit, M.C., Van Reenen, D.D. and Roering C. (1983). Some aspects of the geology, structure and metamorphism of the Southern Marginal Zone of the Limpopo metamorphic complex. *Special Publication of the Geological Society of South Africa*, **8**, 121–142.

Eales, H.V., Marsh, J.S. and Cox, K.G. (1984). The Karoo igneous province: an introduction. *Special Publication of the Geological Society of South Africa* , **13**, 1–26.

Fischer, K.M. (2002). Waning buoyancy in the crustal roots of old mountains. *Nature*, **417**, 933–935.

Griffin, W.L. and O'Reilly, S.Y. (1987). The composition of the lower crust and the nature of the continental Moho. *In*: Nixon, P.H. (Editor), Mantle Xenoliths, *Wiley, London*, *United Kingdom*, 413–430.

Gurrola, H., Minster, J.B. and Owens, T. (1994). The use of velocity spectrum for stacking receiver functions and imaging upper mantle discontinuities. *Geophysical Journal International*, **117**, 427–440.

Gwavava, O., Swain, C.J., Podmore, F. and Fairhead, J.D. (1992). Evidence of crustal thinning beneath the Limpopo Belt and Lebombo monocline of southern Africa based on regional gravity studies and implications for the reconstruction of Gondwana. *Tectonophysics*, **212**, 1–20.

Hales, A.L. (1969). A seismic discontinuity in the lithosphere. *Earth and Planetary Science Letters*, **7**, 44–46.

Holzer, L., Frei, R., Barton, J.M. and Kramers, J.D. (1998). Unravelling the record of successive high-grade events in the Central Zone of the Limpopo Belt using Pb single phase dating of metamorphic minerals. *Precambrian Research*. **87**, 87–115.

Horstwood, M.S.A., Nesbitt, R.W., Noble, S.R. and Wilson, J.F. (1999). U-Pb zircon for an extensive early Archaean craton in Zimbabwe: a reassessment of the timing of craton formation, stabilisation and growth. *Geology*, **27**, 707–710.

James, D.E. (2002). How old roots lose their bounce. *Nature*, **417**, 911–912.

James, D.E., Niu, F. and Rokosky, J. (2003). Crustal structure of the Kaapval Craton and its significance for early crustal evolution. *Litbos*, **71**, 413–429.

Kanasewich, E.R. (1981). Time Sequence Analysis in Geophysics, 3rd Edition. *The University of Alberta Press, Canada*, 480pp.

Kamber, B.S., Blenkinsop, T.G., Villa, I.M. and Dahl, P.S. (1995a). Proterozoic transpressive deformation in the Northern Marginal Zone, Limpopo Belt, Zimbabwe. *Geology*, **103**, 493–508.

Kamber, B.S., Kramers, J.D., Napier, R., Cliff, R.A. and Rollinson, H.R. (1995b). The Triangle Shearzone, Zimbabwe, revisited: new data document an important event at 2.0 Ga in the Limpopo Belt. *Precambrian Research*, **70**, 191–213.

Kennett, B.L.N. and Engdahl, E.R. (1991). Travel times for global earthquake location and phase identification. *Geophysical Journal International* , **105**, 429–465.

Key, R. M. and Hutton, S.M. (1976). The tectonic generation of the Limpopo Mobile Belt and a definition of its western extremity. *Precambrian Research*, **3**, 79–90.

Kreissig, K., Nägler, Th. F., Kramers, J.D., van Reenen, D.D. and Smit, C.A. (2000). An Isotopic and geochemical study of the northern Kaapvaal Craton and the Southern Marginal Zone of the Limpopo Belt: Are they juxtaposed terranes? *Litbos*, **50**: 1–25.

Langston, C.A. (1979). Structure under Mount Rainier, Washington, inferred from teleseismic body waves. *Journal of Geophysical Research*, **84**, 749–762.

Last, R.L., Nyblade, A.A. and Langston, C.A. (1997). Crustal structure of the East African Plateau from receiver functions and Rayleigh wave phase velocities. *Journal of Geophysical Research*, **102**, 24469–24483.

McCourt, S. and Armstrong, R.A. (1998). SHRIMP U-Pb zircon geochronology of granites from the Central Zone, Limpopo Belt, southern Africa: Implications for the age of the Limpopo Orogeny. *South African Journal of Geology*, **101**, 329–338.

Mkweli, S., Kamber, B. and Berger, M. (1995). Westward continuation of the craton-Limpopo Belt tectonic break in Zimbabwe and new age constraints on the timing of the thrusting. *Journal of the Geological Society of London*,

152, 77—83

Mukasa, S.B., Wilson, A.H. and Carlson, R.W. (1998). A multielement geochronologic study of the Great Dyke, Zimbabwe: significance of the robust and reset ages. *Earth and Planetary Science Letters*, **164**, 353–369.

Nägler, Th.F., Kramers, J.D., Kamber, B.S., Frei, R. and Prendergast, M.D.A. (1997). Growth of subcontinental lithospheric mantle beneath Zimbabwe started at or before 3.8 Ga: Re-Os study on chromites. *Geology*, **25**, 983–986.

Nguuri, T.K., Gore, J., James, D.E., Wright, C., Zengeni, T.G., Gwavava, O., Webb, S.J. and Snoke, J.A. (2001). Crustal structure beneath southern Africa and its implications for the formation and evolution of the Kaapvaal and Zimbabwe Cratons. *Geophysical Research Letters*, **28**, 2501–2504.

Niu, F. and James, D.E. (2002). Fine structure of the lowermost crust beneath the Kaapvaal Craton and its implications for crustal formation and evolution. *Earth and Planetary Science Letters*, **200**, 121–130.

Owens, T.J., Zandt, G. and Taylor, S.R. (1984). Seismic eveidence for an ancient rift beneath the Cumberland Plateau, Tennessee: a detailed analysis of broadband teleseismic P waveforms. *Journal of Geophysical Research*, **89**, 7783–7795.

Owens, T.J., Taylor, S.R. and Zandt, G. (1987). Crustal structure at regional seismic test network stations determined from inversion of broadband teleseismic P waveforms. *Bulletin of the Seismological Society of America*, **77**, 631–662.

Paulssen, H., Visser, J. and Nolet, G. (1993). The crustal structure from teleseismic P-wave coda – 1. Method. *Geophysical Journal International,* **112**, 15–25.

Ridley, J. (1992). On the origins and tectonic significance of the charnockite suite of the Archaean Limpopo Belt, Northern Marginal Zone, Zimbabwe. *Precambrian Research*, **55**, 407–427.

Rollinson, H.R. (1993). A terrane interpretation of the Archaean Limpopo Belt. *Geological Magazine*, **130**, 755–765.

Rollinson, H.R. and Blenkinsop, T. (1995). The magmatic, metamorphic and tectonic evolution of the Northern Marginal Zone of the Limpopo Belt in Zimbabwe. *Journal of the Geological Society of London*, **152**, 65–75.

Savage, M.K. (1999). Seismic anisotropy and mantle deformation: what have we learned from shear wave splitting? *Reviews of Geophysics*, **37**, 65–106.

Schaller, M., Steiner, O., Studer, I., Holzer, L., Herwegh, M. and Kramers, J.D. (1999). Exhumation of Limpopo Central Zone granulites and dextral continent-scale transcurrent movement at 2.0 Ga along the Palala Shear Zone, Northern Province, South Africa. *Precambrian Research*, **96**, 263–288.

Stuart, G.W. and Zengeni, T.G., 1987. Seismic crustal structure of the Limpopo mobile belt, Zimbabwe. *Tectonophysics*, **144**, 323–335.

Van Reenen, D.D., Barton, J.M., Roering, C., Smith, C.A. and Van Schalkwyk, J.F. (1987). Deep crustal response to continental collision: the Limpopo Belt of southern Africa. *Geology*, **15**, 11–14.

Van Reenen, D.D., McCourt, S. and Smit, C.A. (1995). Are the Southern and Northern Marginal Zones of the Limpopo Belt related to a single continental collisional event? *South African Journal of Geology*, **98**, 498–504.

Watkeys, M.K. (1983). Brief explanatory notes on the provisional geological map of the Limpopo Belt and environs. *Special Publication of the Geological Society of South Africa*, **8**, 5–8.

Watkeys, M.K., Light, M.P.R. and Broderick, T.J. (1983). A retrospective view of the Central Zone of the Limpopo Belt, Zimbabwe. *Special Publication of the Geological Society of South Africa*, **8**, 65–80.

White, R. and McKenzie, D. (1989). Magmatism at rift zones: the generation of volcanic continental margins and flood basalts. *Journal of Geophysical Research*, **94**, 7685–7729.

Wilson, J.F. (1990). A craton and its cracks: some of the behaviour of the Zimbabwe Block from late Archaean to the Mesozoic in response to horizontal movements, and the significance of some of its mafic dyke fracture patterns. *Journal of African Earth Sciences*, **10**, 483–501.

Zandt, G. and Ammon, C.J. (1995). Continental crust composition constrained by measurements of crustal Poisson's ratio. *Nature*, **374**, 152–154.

Zandt, G., Myers, S.C. and Wallace, T.C. (1995). Crust and mantle structure across the Basin and Range-Colorado plateau boundary at 37°N latitude and implications for Cenozoic extensional mechanism. *Journal of Geophysical Research*, **100**, 10529–10548.

Editorial handling: P.H.G.M. Dirks